Rock Mech. Rock Engng. (2006) 39 (3), 185–213
DOI 10.1007/s00603-005-0065-4

Rock Mechanics and Rock Engineering
Printed in Austria

Hydromechanical Behaviour of Fontainebleau Sandstone

By

J. Sulem and **H. Ouffroukh**

CERMES – Ecole Nationale des Ponts et Chaussées/LCPC, Institut Navier, Marne-La-Vallée, France

Received December 20, 2004; accepted May 10, 2005
Published online August 19, 2005

Summary

The hydromechanical behaviour of Fontainebleau sandstone is studied on the basis of isotropic and triaxial compression tests in drained and undrained conditions on water saturated samples. The effect of the evolution of the compressibility of the rock with the applied stress on the poromechanical parameters is shown. On the basis of micro-mechanical considerations, a new expression for the Skempton coefficient B is proposed as a function of the porosity, the drained bulk compressibility and the grain and fluid compressibility. The relation between rock deformation and pore-pressure evolution in undrained deviatoric tests is analysed. An elasto-plastic constitutive model with stress-dependent elasticity and damage is proposed to describe the behaviour of the rock and validated through back analysis of drained and undrained tests.

Keywords: Sandstone, poromechanics, undrained deformation, non-linear elasticity, plasticity.

1. Introduction

The effect of interstitial fluid on the behaviour of porous rocks is commonly studied experimentally using drained triaxial compression tests i.e. at constant imposed pore pressure (e.g. Robinson, 1959; Handin et al., 1963; Boozer et al., 1963; Lane, 1969; Cornet, 1977). A relatively small number of experimental studies of the response of rocks in undrained conditions have been published in the literature due to the difficulty of performing such tests on rock samples with precise measurement of pore pressure evolution (e.g. Merritt and Aldrich, 1969; Mesri et al., 1976; Dropek and Johnson, 1978; Tien et al., 1988; Streiger and Leung, 1991; Fredrich et al., 1995; Fabre and Gustkiewicz, 1997; Archambault et al., 1999; Bouteca and Gueguen, 1999). The usefulness of Terzaghi's effective stress principle for describing failure criteria for rocks was demonstrated in numerous experimental investigations. On the other hand it is

well admitted that stress-strain relationships should be formulated in terms of a modified effective pressure expressed as the difference between the total stress and the pore pressure multiplied by a coefficient b with values between 0 and 1 (Garg and Nur, 1973; Lade and De Boer, 1997; Gustkiewicz, 1998). In the regime of linear elasticity of isotropic rocks, this coefficient can be precisely determined (Nur and Byerlee, 1971) and is equal to the so-called Biot coefficient $b = 1 - K/K_s$ where K is the (drained) elastic compression modulus of the rock matrix and K_s is the elastic compression modulus of the solid phase.

In this paper, the hydro-mechanical behaviour of Fontainebleau sandstone is studied on the basis of an experimental program of triaxial compression tests in drained and undrained conditions. A specific experimental setting has been used for reliable monitoring of deformation and pore pressure. Contacts between the sample and the loading platens are lubricated to avoid end friction problems. In addition loading-unloading cycles are performed at various levels of the applied load for a proper evaluation of the elastic properties. Emphasis is given to the pressure dependent character of the poro-elastic material properties. The experimental results are used for the calibration of an elasto-plastic constitutive model for granular rocks with stress dependent elasticity and damage. Special attention is devoted to the study of pore pressure evolution and its influence on rock deformation.

2. Experimental Setting

A triaxial cell with internal diameter of 140 mm is used (Fig. 1). This cell, which can sustain a confining pressure up to 60 MPa, contains a system of hydraulic self-compensated piston. The loading piston is then equilibrated during the confining pressure build up and directly applies the deviatoric stress. The axial and radial strains are measured directly on the sample inside the cell with two axial transducers and four radial ones of LVDT type (see section AA on Fig. 1 and Fig. 2). These internal devices allow to avoid the main errors of strain measurements of devices external to the cell such as the compliance of the loading device, the tilting of the specimen, the bedding errors at the ends of the specimen. This device is also more adequate than strain gages which are currently used for strain measurements on rocks. Strain gages can perturb the porous specimen because of glue penetration inside the sample and are useless beyond the onset of strain localisation. A correction for the radial deformation of the membrane during the test has been calibrated. The lower base of the cell is equipped with a pore pressure transducer. Pore pressure measurements during test are then performed very close to the sample base. The confining pressure is applied by a servo controlled high pressure generator which consists of a piston moving in a pressure chamber. The pressure generator is guided by an electronic regulator receiving an analogical signal from an external transducer. The regulators are programmed by a PC computer.

Axisymmetric strain-controlled compression tests in drained and undrained conditions have been performed on Fontainebleau sandstone at various confining pressures (7, 14, 28, 40 and 50 MPa). The axial displacement is servo-controlled via the internal *radial* transducers at a rate corresponding to a constant radial strain rate

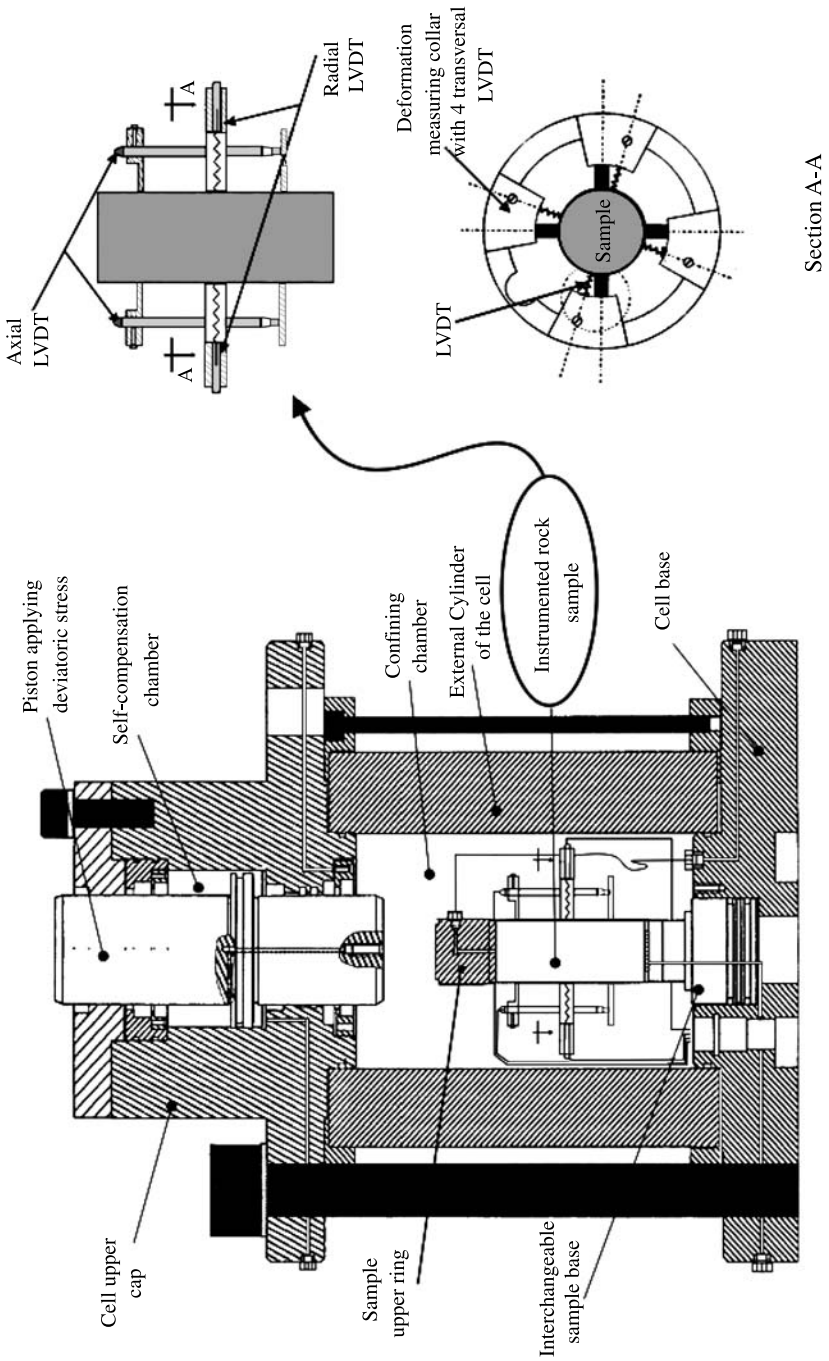

Fig. 1. Testing device

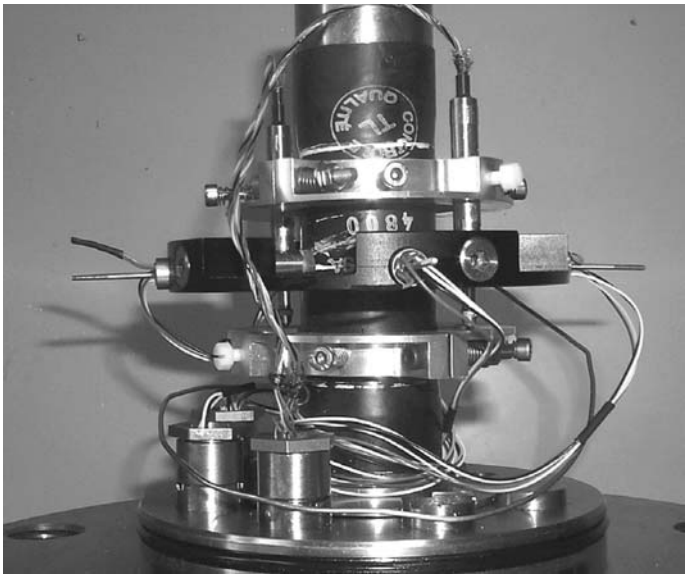

Fig. 2. Instrumentation of the sample inside the cell

of $10^{-5}\,\mathrm{sec}^{-1}$ which is slow enough to insure fully drained deformation of porous sandstone. The choice of the radial strain measurements for the servo-control of the test is made because the radial strains are increasing rapidly close to the peak. This choice results in an imposed axial strain rate which is decreasing close to the peak strength. The tests have been stopped close after the maximum axial load (peak strength) has been reached.

Failure along a unique shear band is obtained for confined tests at low confining pressure and eventually along several bands for tests at high confining pressure. The interface between the rock specimen and the loading platens of the testing machine is lubricated to avoid friction (Labuz and Bridell, 1993; Pellegrino et al., 1997; Papamichos et al., 2000; El Bied and Sulem, 2003). Cylindrical specimens with a diameter of 37.5 mm and a height of 77 mm are used.

The rock chosen for this study is the Fontainebleau sandstone with a porosity of 21%. It is a uniformly graded rock with a grain size of 0.25 mm. Its composition is 99.8% quartz. Due to the remarkable homogeneity and isotropy of this rock, Fontainebleau sandstone has been used in many previous studies (e.g. Bourbie et al., 1987; David and Darot, 1989; Fredrich et al., 1993; Haied and Kondo, 1997; El Bied et al., 2001).

3. Hydrostatic Compression Tests

The aim of this section is to study the stress dependent character of the poro-elastic parameters of granular rocks with relatively high porosity such as Fontainebleau sandstone. Hydrostatic compression tests in drained and undrained conditions have

Table 1. Hydrostatic compressions tests

Sample reference	Test reference	Initial back pressure (MPa)	Initial confining pressure (MPa)	Final confining pressure (MPa)	Final pore pressure (MPa)	Drainage conditions
G13	S13d	2	2.5	52.5	34.7	undrained
	S13b	2	4.5	52	31	undrained
	S13c	2	7.5	53.7	23	undrained
	S13e	2	12.5	52	19.6	undrained
	Co13	2	2.5	58	2	drained
G16	S16a	2	2.5	52	38.6	undrained
	S16b	2	4.5	52	31	undrained
	S16c	2	12.5	52	23	undrained
	Co16	2	2.5	42	2	drained
G20	S20	2	2.5	29	19.4	undrained
	Co20	2	2.5	42	2	drained

been performed on water saturated samples (Table 1). To insure a good saturation of the samples, de-aired water is circulated inside the sample, then a back pressure of 2 MPa is applied. For drained tests, this back pressure is kept constant whereas for undrained test, no water exchange is allowed between the sample and the exterior.

3.1 Drained Tests

The response for drained tests is shown on Fig. 3 for three different samples. On Fig. 3a the axial strain ($\varepsilon_{\text{axial}}$), the radial strain ($\varepsilon_{\text{radial}}$), and the volumetric strain ($\varepsilon_{\text{volumetric}} = \varepsilon_{\text{axial}} + 2\varepsilon_{\text{axial}}$) are plotted versus the confining pressure. We observe some difference in the axial and the radial deformation which could be attributed to the bedding anisotropy of the rock. However this anisotropy is quite weak and observed here at very small strains.

It is observed that the initial part of the stress-strain curve is convex (Fig. 3b). This is commonly observed for sandstones (e.g. Zimmerman, 1991; Sulem et al., 1999). The stress dependency of the elastic compression modulus is, from a micro-mechanical point of view, attributed to closing of the existing micro-cracks. The secant bulk modulus is represented on Fig. 3c. Accordingly it is increasing with increasing effective stress. However the data show that at high confining pressure (>40 MPa) the bulk modulus reaches a maximum and starts to decrease which can be attributed to the onset of pore collapse.

3.2 Undrained Tests

In order to study the effect of confining pressure on the response of the rock in undrained hydrostatic compression the following loading path has been imposed: from an initial value of 2.5 MPa, a loading-unloading cycle in undrained conditions up to a maximum total confining pressure of 50 MPa is performed; at the end of this cycle, the confining pressure is raised to a higher value (4.5 MPa) in drained conditions and a new loading-unloading cycle in undrained conditions is performed;

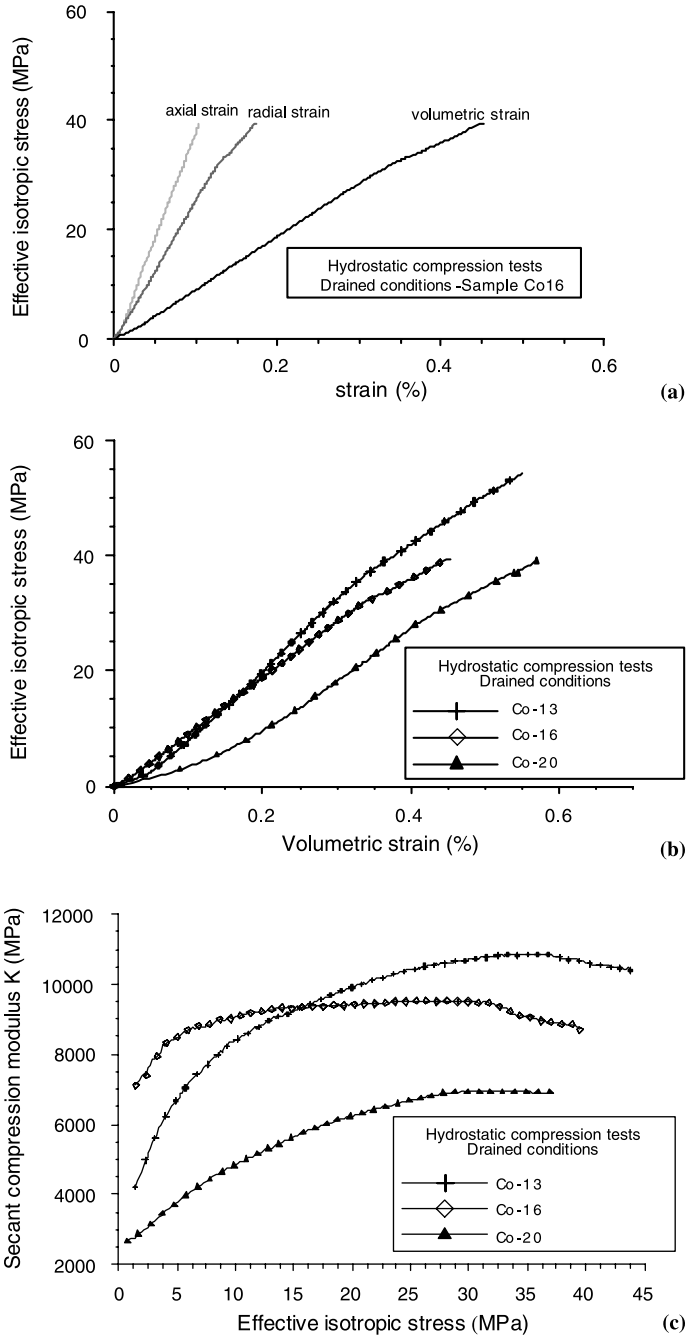

Fig. 3. Hydrostatic compression tests in drained conditions: **a** radial, axial and volumetric response (Co-16); **b** volumetric response; **c** secant compression modulus

the same operation is repeated with an initial confining pressure of 7.5 MPa, then of 12.5 MPa (Table 1).

For porous rocks deformed in the elastic regime, it is generally admitted that Biot's definition of effective stress σ' (Eq. (1)) is more appropriate than Terzaghi effective stress (Nur and Byerlee, 1971):

$$\sigma' = \sigma - bu, \tag{1}$$

where σ is the total stress (positive in compression), u is the pore pressure and b is the so-called Biot coefficient determined by the (effective) compression modulus of the water saturated rock K and the compression modulus of its solid phase K_s

$$b = 1 - \frac{K}{K_s}. \tag{2}$$

The response in terms of generated pore-pressure versus the total confining stress is shown on Fig. 4a, b, c for samples G13, G16 and G20 respectively. The slope of these curves gives Skempton coefficient B:

$$B = \frac{\Delta u}{|\Delta \sigma|}. \tag{3}$$

It is observed that the measured Skempton coefficient is decreasing with increasing initial confining pressure which shows the pressure sensitive character of B. Similar observation has been made by Fredrich et al. (1995) for highly porous rocks.

The total stress-volumetric strain response is shown on Fig. 5. Note that due to the fact that the fluid compressibility ($4.0 * 10^{-4}\,\mathrm{MPa}^{-1}$ at 20 °C) and the quartz grain compressibility ($2.75 * 10^{-5}\,\mathrm{MPa}^{-1}$) are comparable to the saturated rock compressibility ($10^{-4}\,\mathrm{MPa}^{-1}$), undrained tests are not isochoric (i.e. at constant volume) as in classical Soils Mechanics. The undrained stress-strain response in terms of Biot effective stress is shown on Fig. 6 and compared with the response of the drained tests. This graph shows a consistent response for the different drainage conditions. The effective and the undrained bulk moduli K' and K_u are reported on Table 2. The effective bulk modulus obtained from undrained tests K' is close to the drained bulk modulus K.

The undrained tests also exhibit a convex initial part of the effective stress-strain curve when the initial confining pressure is small (tests S13d and S20) which shows that although pore pressure is increasing, the closure of micro-cracks under stress is not totally inhibited.

An expression for the Skempton coefficient B can be derived from micromechanical considerations. The volume V of the sample consists of the volume V_s of the solid phase and the volume V_v of the voids.

$$V = V_s + V_v. \tag{4}$$

The volumetric strain $\Delta\varepsilon_v$ is written as

$$\Delta\varepsilon_v = \frac{\Delta V}{V} = \frac{\Delta V_s}{V} + \frac{\Delta V_v}{V} = (1-n)\frac{\Delta V_s}{V_s} + n\frac{\Delta V_v}{V_v}. \tag{5}$$

For fully saturated porous rocks the interconnected void space is fully occupied by water ($V_w = V_v$, where V_w is the volume occupied by the fluid).

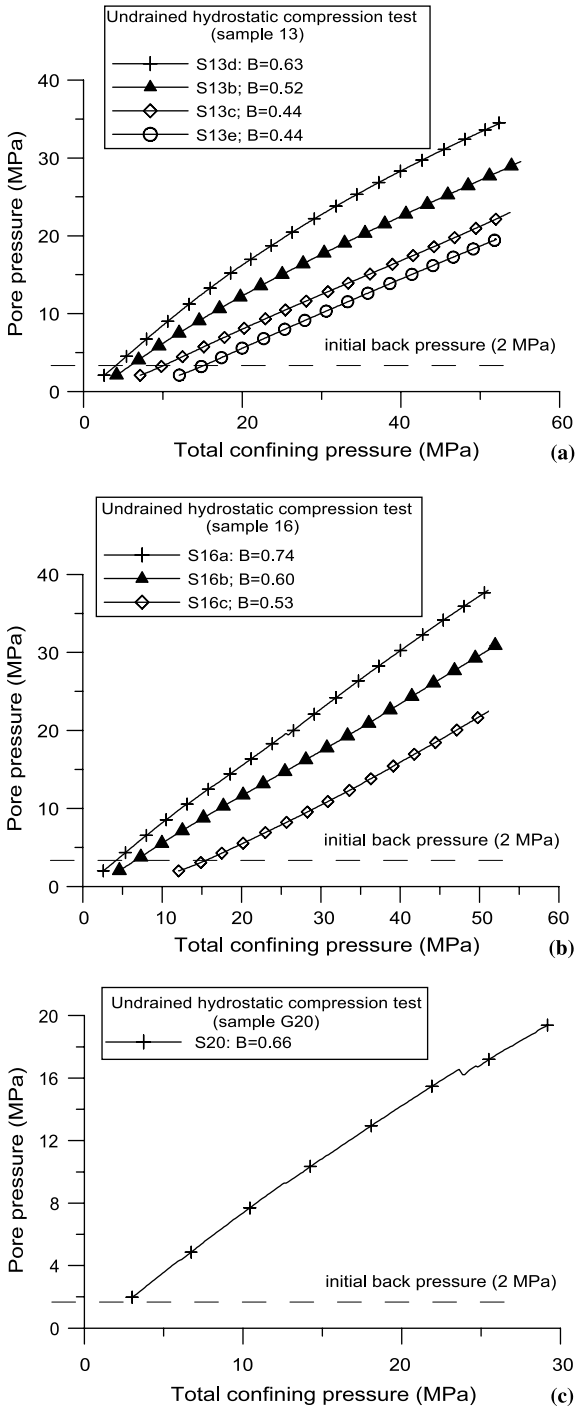

Fig. 4. Pore pressure generation for undrained hydrostatic compression tests

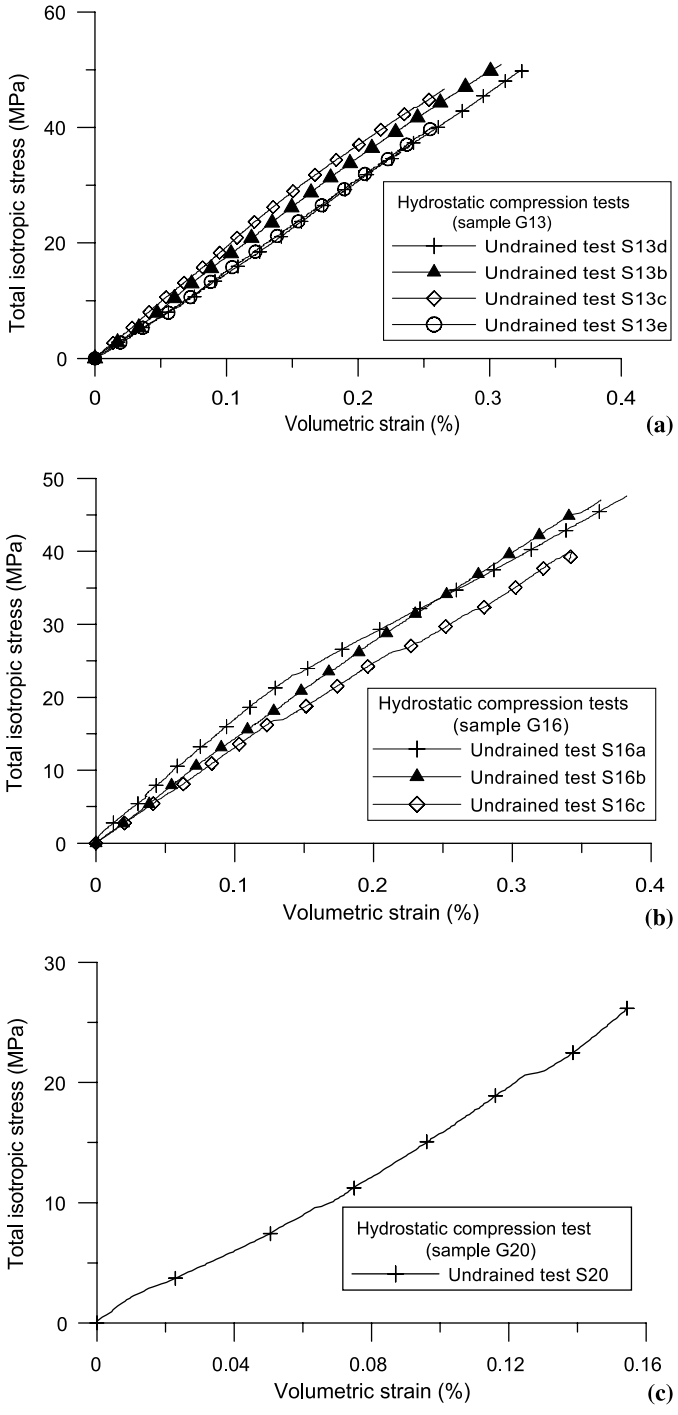

Fig. 5. Hydrostatic compression tests: Volumetric response in undrained conditions

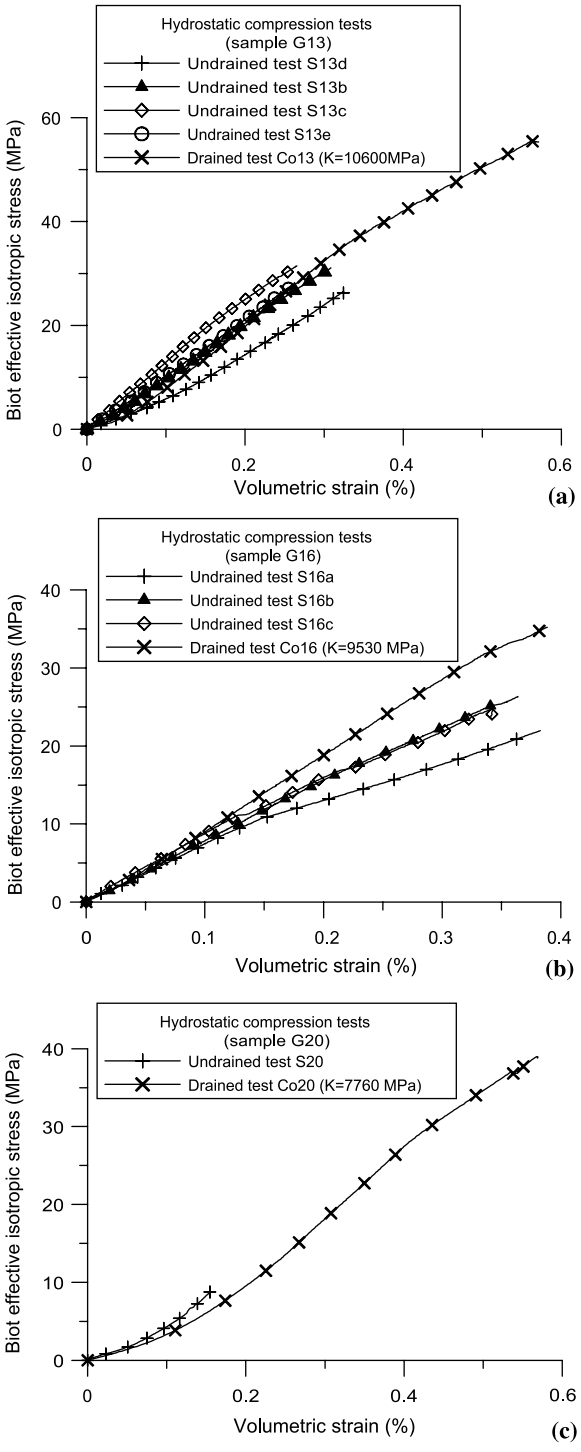

Fig. 6. Hydrostatic compression tests: Volumetric response in drained and undrained conditions

Table 2. Compression moduli in drained and undrained hydrostatic tests

Sample reference	Test reference	Drainage conditions	Effective average compression modulus K (MPa)	Undrained average compression modulus K_u (MPa)
G13	S13d	undrained	8400	15534
	S13b	undrained	10400	16844
	S13c	undrained	12100	17870
	S13e	undrained	10800	15816
	Co13	drained	10600	
G16	S16a	undrained	5554	11933
	S16b	undrained	7360	13017
	S16c	undrained	7000	11380
	Co16	drained	9530	
G20	S20	undrained	9145	16000
	Co20	drained	7760	

The volumetric deformation of the pore fluid and of the solid phase can be expressed as

$$\frac{\Delta V_v}{V_v} = \frac{\Delta u}{K_w}, \qquad \frac{\Delta V_s}{V_s} = \frac{\Delta \sigma'}{K_s}, \tag{6}$$

where K_w is the compression modulus of the pore fluid ($K_w = 2028$ MPa, for de-aired water at a temperature of 20 °C) and K_s is the compression modulus of the solid phase ($K_s = 36000$ MPa, for quartz grains).

For simplification, we assume here that the Taylor's (1948) intergranular stress coincide with Biot's effective stress.

With

$$\Delta \varepsilon_v = \frac{\Delta \sigma'}{K} = \frac{\Delta \sigma - b \Delta u}{K}, \tag{7}$$

the excess pore pressure is expressed from Eq. (5) as

$$\Delta u = \frac{\left(\frac{1}{K} - \frac{1-n}{K_s}\right)}{\left(\frac{n}{K_w} - b\frac{1-n}{K_s} + \frac{b}{K}\right)} \Delta \sigma. \tag{8}$$

Consequently the following expression for the Skempton coefficient B is obtained

$$B = \frac{\left(\frac{1}{K} - \frac{1-n}{K_s}\right)}{\left(\frac{n}{K_w} - b\frac{1-n}{K_s} + \frac{b}{K}\right)}. \tag{9}$$

The above expression is different from the one proposed by Bishop (1973) which reads as follows:

$$B = \frac{\left(\frac{1}{K} - \frac{1}{K_s}\right)}{\left(\frac{1}{K} - \frac{1}{K_s}\right) + n\left(\frac{1}{K_w} - \frac{1}{K_s}\right)}. \tag{10}$$

On the other hand, the pore pressure excess Δu can be expressed using the undrained compression modulus K_u which can be evaluated on the experimental data (Fig. 5, Table 2):

$$\Delta u = \frac{1}{b}(\Delta\sigma - \Delta\sigma') = \frac{K_u - K}{b}\Delta\varepsilon_v = \frac{K_u - K}{bK_u}\Delta\sigma, \tag{11}$$

resulting in the following expression for B as function of the various compression moduli K, K_u, and K_s

$$B = \frac{K_u - K}{bK_u} = \frac{K_u - K}{(1 - K/K_s)K_u}. \tag{12}$$

On Fig. 7 the computed expression for the Skempton coefficient B (Eq. (9)) is plotted versus the effective compression modulus K and compared with the measured values. On the same graph, the value of B computed with Bishop's expression (Eq. (10)) and the one evaluated from expression (12) are also plotted. As observed by other authors (e.g. Fredrich et al., 1995), the B values decrease with increasing compression modulus. We notice that Bishop's expression underestimates the values of B whereas the expression proposed in Eq. (9) leads to computed values in good accordance with the measured ones. The B values calculated from Eq. (12) also match correctly the measurements. These results demonstrate the efficiency of the experimental setting for pore pressure and strains measurements.

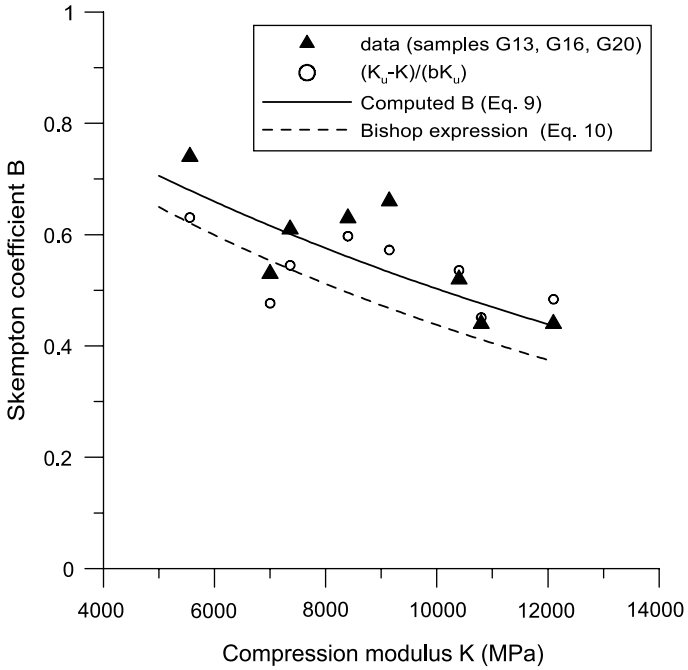

Fig. 7. Computed and measured Skempton coefficient

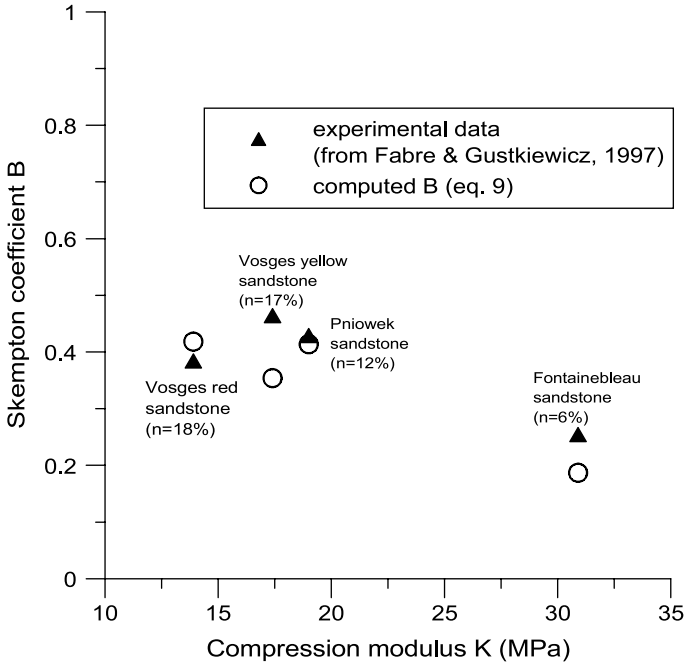

Fig. 8. Computed Skempton coefficient compared with experimental data from Fabre and Gustkiewicz (1997)

On Fig. 8 the value of B coefficient measured on other types of sandstone with different porosity published by Fabre and Gustkiewicz (1997) are compared with the computed values obtained with Eq. (9). This graph shows a good agreement between computed and measured values.

4. Deviatoric Compression Tests

4.1 Stress-Strain Response

In the range of confining pressures used in our tests the behaviour of Fontainebleau sandstone is rather brittle. For the various confining pressures (7 MPa, 14 MPa, 28 MPa, 40 MPa and 50 MPa) the tests have been stopped just after the peak of axial load. The corresponding axial strain is around 0.5% for low confining pressure and 1% for higher ones. The overall axial stress response is presented on Fig. 9 for drained tests and on Fig. 10 for undrained tests. On these graphs, negative (respectively positive) volumetric strains correspond to contractant (respectively dilatant) behaviour. The samples undergo initial compaction and then dilatant strain hardening. The contractant phase is less pronounced for undrained tests due to pore pressure generation.

As pointed in the introduction Terzaghi's effective stress is appropriate for describing failure criteria for rocks. Accordingly, on Fig. 11 the maximum axial (Terzaghi)

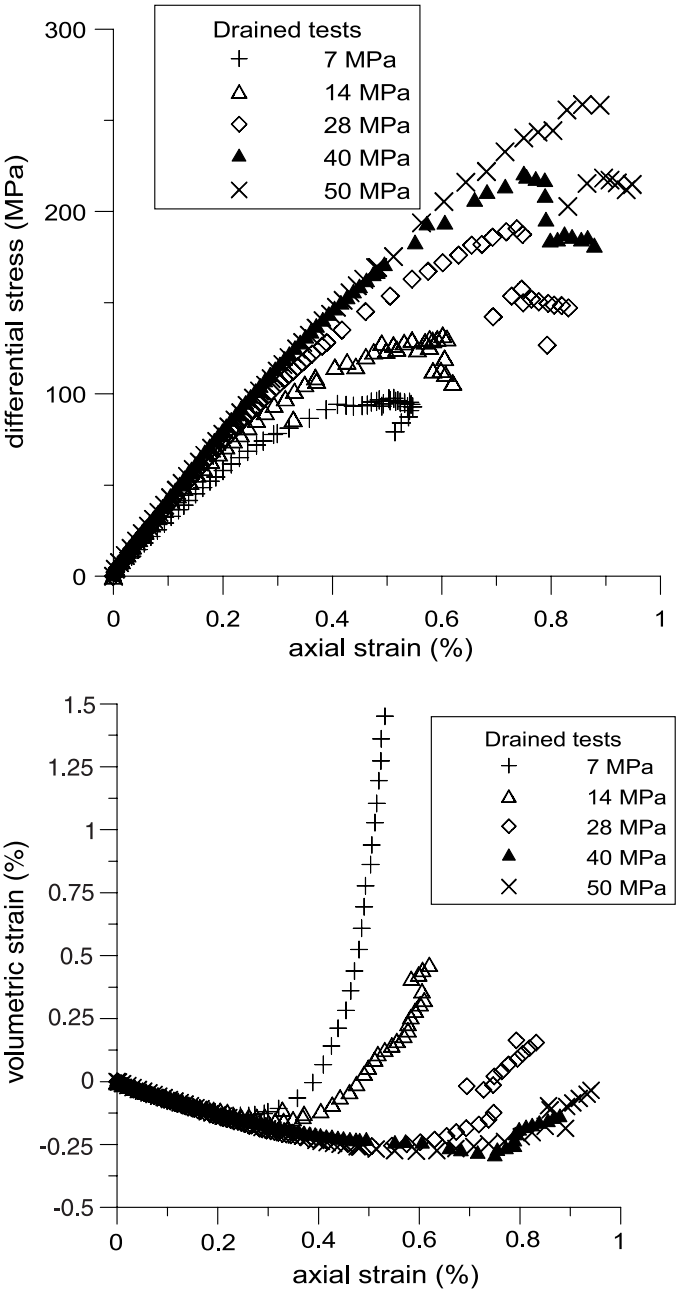

Fig. 9. Drained tests: Deviatoric stress and volumetric strain versus axial strain

effective stress is plotted versus the (Terzaghi) effective confining pressure. The maximum effective stress is increasing with effective confining pressure. The experimental results for drained and undrained tests on saturated samples are consistent with

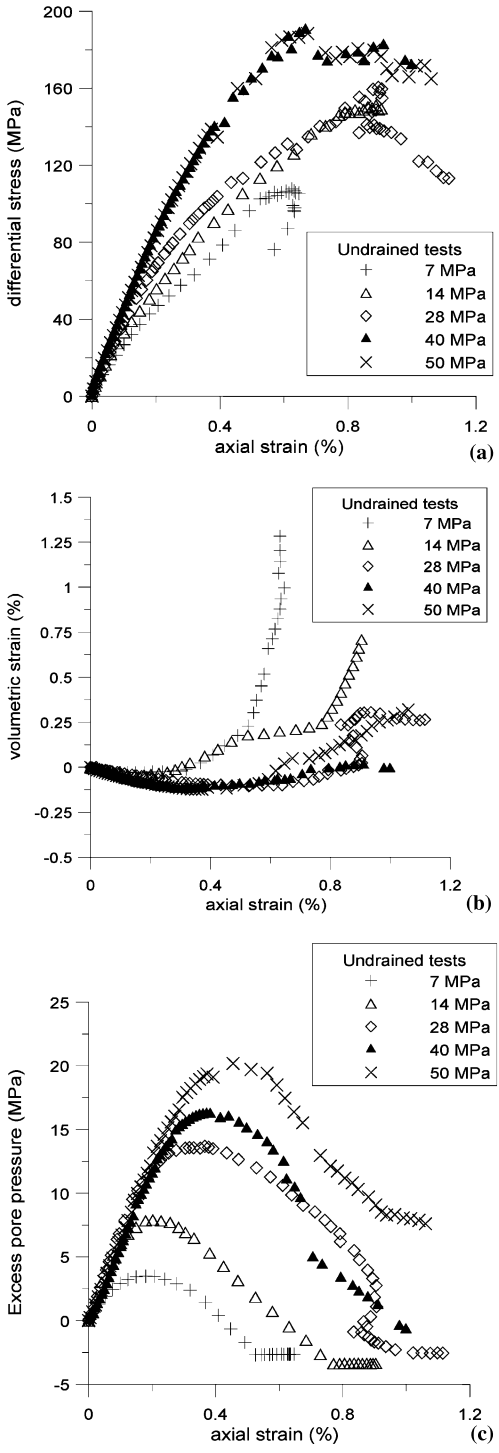

Fig. 10. Undrained tests: Deviatoric stress. volumetric strain and pore pressure versus axial strain

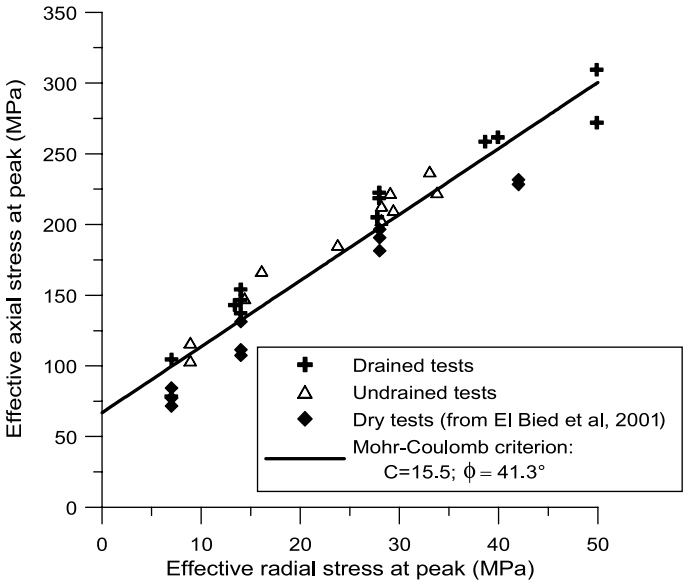

Fig. 11. Failure criterion for drained and undrained tests

those presented in El Bied et al. (2001) for dry samples (Fig. 11). The effective yield stress can be fitted with a linear Mohr-Coulomb criterion

$$\sigma'_{\text{axial}} = 2c\tan(\pi/4 + \phi/2) + \sigma'_{\text{radial}}\tan^2(\pi/4 + \phi/2) \tag{13}$$

with

$$c = 15.5\,\text{MPa} \quad \text{and} \quad \phi = 41.3\,^\circ. \tag{14}$$

4.2 Pore Pressure Generation in Undrained Tests

The generated pore-pressure in undrained tests is plotted versus the axial strain for the various confining pressures on Fig. 10c. Theses curves are consistent with the volumetric response of the samples (Fig. 10b). They exhibit a maximum at the critical state of transition between contractant and dilatant volumetric strain. This maximum increases with increasing confining pressure. At low confining pressures (7 and 14 MPa) the pore pressure at yield effective stress is lower than the initially applied back pressure. Such cavitation phenomenon has been observed for dense sand (Roger et al., 1998) and for sandstone under low confining pressure (Tien et al., 1988).

5. Constitutive Model

5.1 Basic Features of the Constitutive Model

The experimental results presented above have shown the importance of the pressure-dependent character of the behaviour of porous sandstone. This is reflected in the

drained hydrostatic tests by the effect of the confining stress on the bulk modulus of the rock and in the undrained hydrostatic tests by the effect of the confining stress on the Skempton coefficient. The deviatoric compression tests confirmed that Fontainebleau sandstone elasticity is not only stress-dependent but also coupled to the plasticity. Stress dependency of the elastic moduli can account for an initially convex upward stress-strain curve in hydrostatic or uniaxial compression, which is, from a micro-mechanical point of view, attributed to closing of the cracks. Mathematically this effect can be modelled by assuming an appropriate complementary energy density function, which plays the role of an elastic strain potential and leads to a hyperelastic model. In addition, rock elasticity degrades in due course of deformation due to micro-crack generation. This phenomenon can be described mathematically by introducing plastic strain as an additional internal variable into the appropriate state function (e.g. the free energy).

Within the frame of plasticity theory, the experimental data clearly support a mixed hardening/softening model. In particular one finds very good agreement with the following assumption: the plastic shearing strain intensity is a good macroscopic measure of plastic slip which occurs at intergranular boundaries and across micro-cracks. Past the state of initial yield, friction is mobilised as function of plastic shear strain and reaches saturation at some given peak value. On the other hand, in due course of deformation new microcracks may be activated and/or new ones may form. We therefore assume that all deviatoric softening must be attributed to microcracking, which leads to a decrease of the tensile strength. This softening mechanism may be active during all stages of straining processes. However it becomes more pronounced when the material looses its capacity to mobilise additional friction resistance. Thus for simplicity we assume that during the friction hardening phase all tensile strength softening is negligible and it becomes noticeable only past the peak of the mobilised friction.

Concerning plastic volumetric strains, the experimental data show that at low confining pressures the rock dilates strongly whereas at higher confining pressures rock dilatancy diminishes. This pressure sensitivity of the plastic volumetric strains indicates that they must be generally split into a part due to dilatancy and a part due to compaction (grain slip and rotation with partial grain crushing). In this model the effect of compaction is lumped together with the effect of dilatancy, and accordingly plastic volume changes are assumed to be solely linked to plastic-frictional yield. Thus we postulate a constitutive constraint between plastic volumetric and plastic shear strain increments.

Emphasis is given on the calibration strategy of the constitutive model which is solely done on the basis of *drained* compression triaxial tests. The validation of the model is done by back analysis of the experimental data both in drained and undrained conditions.

We use here the constitutive model proposed by Sulem et al., 1999 for granular rocks. This model which is described and validated here for axisymmetric triaxial stress states has been also used and validated for hollow cylinders (Papamichos, 1999) with a very good prediction of the hollow cylinder response. In the previous studies drained conditions have been considered. The model is extended here to account for pore pressure generation in undrained conditions.

5.2 Stress-dependent Elasticity and Damage

Stress-dependent elasticity has been observed in the experiments on Fontainebleau sandstone. Accordingly, the elastic shear modulus G and compression modulus K are assumed to depend on both the mean stress $p = \sigma_{kk}/3$, and the second invariant of the deviatoric stress tensor $T = \sqrt{s_{ij}s_{ij}/2}$ where σ is the stress tensor and s its deviator.

$$G = G(p, T); \qquad K = K(p, T) \tag{15}$$

Remark: In Eq. (15) the effect of the third stress invariant is not considered. This could be easily included in the model but due to the lack of experimental data, it is usually not possible to determine its influence on the elasticity of granular rocks.

We assume that the underlying elasticity of the considered rock is a *hyperelasticity*, which is described by the corresponding complementary energy density function

$$w^c(\sigma_{ij}) = \int_0^{\sigma_{ij}} \varepsilon^e_{ij} d\sigma_{ij}. \tag{16}$$

Accordingly w^c is a stress potential function for the elastic strains

$$\varepsilon^e_{ij} = \frac{\partial w^c}{\partial \sigma_{ij}}. \tag{17}$$

The existence of a complementary energy density function guaranties that in arbitrary, closed stress cycles in the elastic domain no energy is produced nor dissipated.

By decomposing the elastic strain in spherical and in deviatoric part the elasticity relationships are written as

$$\varepsilon^e_{kk} = \frac{\partial w^c}{\partial p} = \frac{p}{K}; \qquad e^e_{ij} = \frac{\partial w^c}{\partial T} = \frac{s_{ij}}{2G}, \tag{18}$$

where e is the deviator of the strain tensor.

A necessary and sufficient condition for an elastic material to be hyperelastic is then:

$$\frac{\partial}{\partial T}\left(\frac{p}{K}\right) = \frac{\partial}{\partial T}\left(\frac{\partial w^c}{\partial p}\right) = \frac{\partial}{\partial p}\left(\frac{\partial w^c}{\partial T}\right) = \frac{\partial}{\partial p}\left(\frac{T}{G}\right). \tag{19}$$

Equation (19) was obtained by Loret (1985).

For simplicity we assume that the Poisson's ratio ν is stress-independent and accordingly the shear and compression secant moduli G and K respectively are proportional to each other

$$K = \kappa G; \quad \kappa = \frac{2(1+\nu)}{3(1-2\nu)}, \tag{20}$$

and to the secant Young's modulus E.

From Eqs. (19) and (20) it is obtained that the stress-dependency of the elastic shear modulus G can be expressed as the function of a single stress measure which combines the effect of normal and shear stress and which will be called the *equivalent elastic stress* (Sulem et al., 1999)

$$\sigma_e = \sqrt{3(1-2\nu)p^2 + 2(1+\nu)T^2}. \tag{21}$$

Equation (15) is then simplified as follows:

$$G = G(\sigma_e); \qquad K(\sigma_e) = \kappa G(\sigma_e). \tag{22}$$

In other words, under the assumption that the Poisson's ratio ν is stress-independent, the stress dependency of the elastic shear modulus G as a function of a single stress measure σ_e (Eq. 22) guaranties that the elastic model is hyperelastic.

Elastic deformation of sandstones is characterised by the action of two competing effects: Stressing of the rock due to 'healing', that is due to closing of pre-existing micro-cracks. This is seen clearly in the hydrostatic tests as a increase of the secant bulk modulus and may be called *stress-stiffening* effect. On the other hand straining of the rock leads to 'damage', that is creation of new micro-cracks. This is seen in the deviatoric tests as a decrease of the secant shear modulus, and may be called *strain-damaging* effect. Both effects are counter to each other and go of course hand in hand.

This phenomenon has to be considered for appropriate evaluation of the elastic properties. Equation (22) is consequently modified as follows:

$$G = G^*(\sigma_e)\eta(g^p); \qquad \nu = \nu(g^p), \tag{23}$$

where $\eta(g^p)$ is the so-called damage function with the accumulated plastic shearing strain intensity g^p as a measure of internal damage (Lemaître, 1991).

Remark: As the strain damaging effect is considered through the damage function $\eta(g^p)$ (Eq. (23)), for closed stress cycles *in the elastic domain*, the damage variable g^p is constant and consequently the elastic shear modulus G depends only in the equivalent elastic strain σ_e which guaranties that the underlying elastic model is hyperelastic.

5.3 Plasticity

We use the usual decomposition of the strain tensor ε and its deviator e in elastic and plastic part

$$\varepsilon_{ij} = \varepsilon^e_{ij} + \varepsilon^p_{ij}; \qquad e_{ij} = e^e_{ij} + e^p_{ij}. \tag{24}$$

In the following use will be made of the following invariants:

$v^p = \varepsilon^p_{kk}$: accumulated plastic volumetric strain

$g^p = \sqrt{2e^p_{ij}e^p_{ij}}$: accumulated plastic shearing strain intensity.

The basic constitutive assumptions of the plasticity model are illustrated graphically in Fig. 12 which shows the trace of a Coulomb-type yield surface in a (p, T). The yield surface is depicted in this figure by a straight line

$$F = T - (q - p)f = 0, \tag{25}$$

which intersects the T-axis at a point where we read the actual value of the mobilised cohesion

$$c = qf. \tag{26}$$

Due to the assumed rock behaviour, depicted in this figure, and the above expression for the cohesion, all cohesion hardening is attributed to the mobilisation

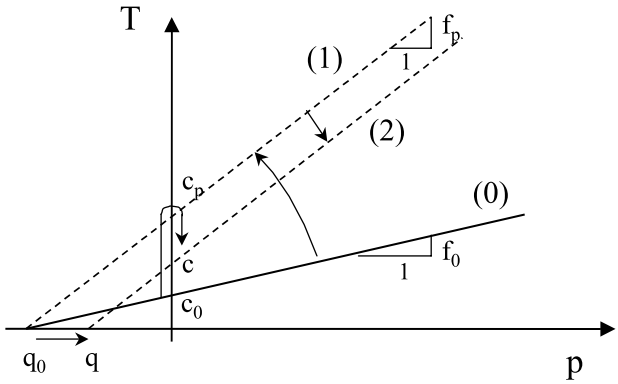

Fig. 12. Motion of the yield surface in stress-space: (*0–1*) 'isotropic' friction-hardening phase; (*1–2*) 'kinematic' softening phase

of internal friction, and all cohesion softening to the degradation of tensile strength, i.e.

$$c = \begin{cases} q_0 f(g^p) & \text{for } 0 \leqslant g^p \leqslant g_p^p \\ f_p q(g^p) & \text{for } g^p \geqslant g_p^p. \end{cases} \tag{27}$$

5.4 Model Calibration on Triaxial Tests Data

In the following the calibration procedure as performed on the pre-peak part of the *drained* triaxial tests is presented.

5.4.1 Elasticity

The starting point of the calibration procedure is the evaluation of the elasticity on the unloading-reloading cycles of the triaxial tests. Although the data are scattered it is clearly observed that Poisson's ratio increases with increasing plastic strain and is accordingly calibrated with the following function (Fig. 13)

$$\nu = \nu_0 + \frac{(g^p)^2}{n_1 + n_2 g^p + n_3 (g^p)^2} \tag{28}$$

with

$$\nu_0 = 0.133; \qquad n_1 = 10^{-10}; \qquad n_2 = 1.2 \times 10^{-3}; \qquad n_3 = 8.4.$$

The secant elastic shear modulus is calibrated with the following function (Fig. 14)

$$\begin{aligned} G_s &= G_s^*(\sigma_e)\eta(g^p) \\ G_s^* &= g_0 + g_1 \sigma_e + g_2 \sigma_e^2 \quad \text{for } \sigma_e \leqslant \sigma_{ep} \\ G_s^* &= G_{sp} \quad \text{for } \sigma_e \geqslant \sigma_{ep} \\ \eta(g^p) &= 1 - \frac{g^p}{\eta_0 + \eta_1 g^p} \end{aligned} \tag{29}$$

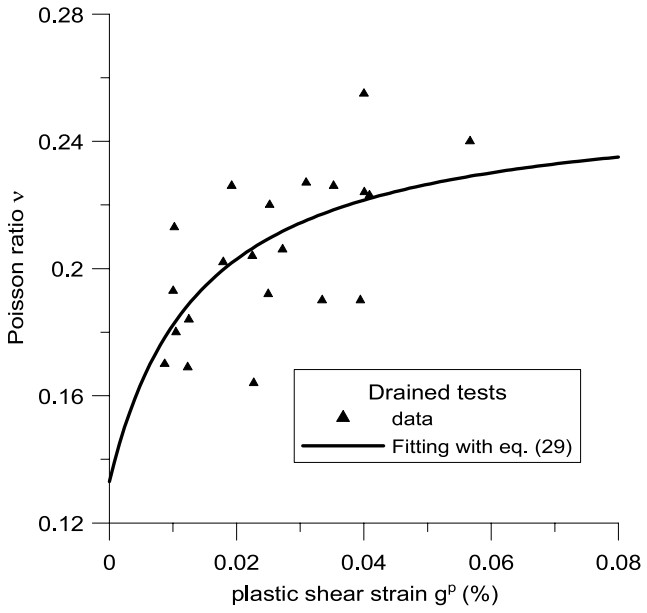

Fig. 13. Drained tests: Evolution of Poisson's ratio with plastic shear strain

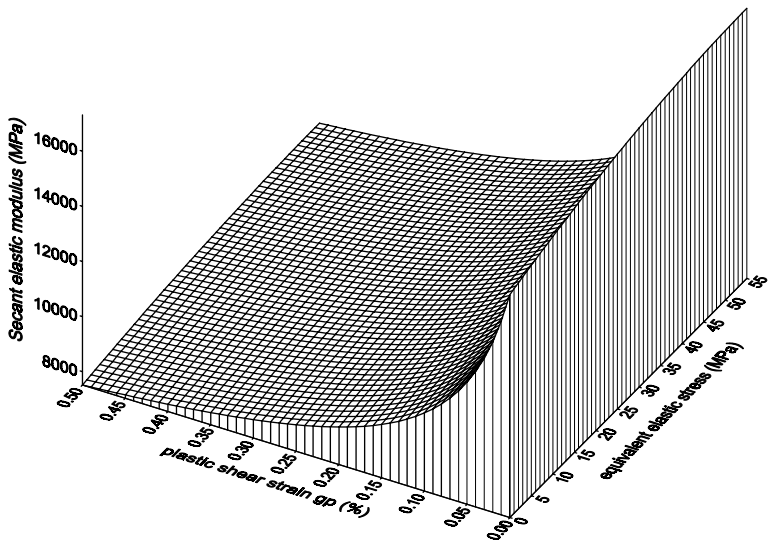

Fig. 14. Drained tests: Evolution of secant elastic shear modulus with stress and plastic strain (Eq. (30)

with

$$g_0 = 15600\,\text{MPa}; \qquad g_1 = 59.3; \qquad g_2 = -0.51\,\text{MPa}^{-1}; \qquad \sigma_{ep} = 58.7\,\text{MPa};$$
$$\eta_0 = 1.3 \times 10^{-3}; \qquad \eta_1 = 1.67.$$

5.4.2 Plasticity

For the drained triaxial compression tests, it is observed that the mobilised friction coefficient increases with accumulated plastic strain up to a maximum value and that this evolution is not significantly affected by the confining pressure (Fig. 15). It is assumed that the tension cut-of q is constant and equal to the value at peak stress, $q = \mathrm{C}/\tan\phi_{\mathrm{peak}} = 17.6\,\mathrm{MPa}$. The mobilised friction coefficient f is thus calibrated as the following function of the plastic shearing strain intensity $\mathrm{g^p}$ (Fig. 14).

$$f(g^p) = f_0 + \frac{(g^p)^2}{f_1 + f_2 g^p + f_3 (g^p)^2}, \tag{30}$$

with

$$f_0 = 0.3; \qquad f_1 = 5.02 \times 10^{-9}; \qquad f_2 = 6.1 \times 10^{-4}; \qquad f_3 = 1.4.$$

In triaxial compression the corresponding friction angle is given by $\sin\phi_m = \frac{3f}{2\sqrt{3}+f}$.

The procedure of calibration of the flow rule is based on the evaluation of the dilatancy parameter $d = \frac{d\varepsilon_v^p}{dg^p}$ on the various tests of the data base (Fig. 16). We observe that the dilatancy parameter depends upon the confining pressure of the considered test. At low confining pressures the rock dilates strongly, whereas at higher confining pressures rock dilatancy diminishes. Consequently a pressure dependent flow rule is calibrated for Fontainebleau sandstone.

Notice that for a good evaluation of the derivative $d = \frac{d\varepsilon_v^p}{dg^p}$, we first curve-fit the experimental data for the plastic volumetric strains at various confining pressures. A hyperbolic law of the form

$$\varepsilon_v^p = \frac{d_1 g^p + d_2 (g^p)^2}{1 + d_3 g^p}; \qquad d = \frac{d\varepsilon_v^p}{dg^p} = \frac{d_1 + 2 d_2 g^p + d_0 d_2 (g^p)^2}{(1 + d_3 g^p)^2} \tag{31}$$

is used.

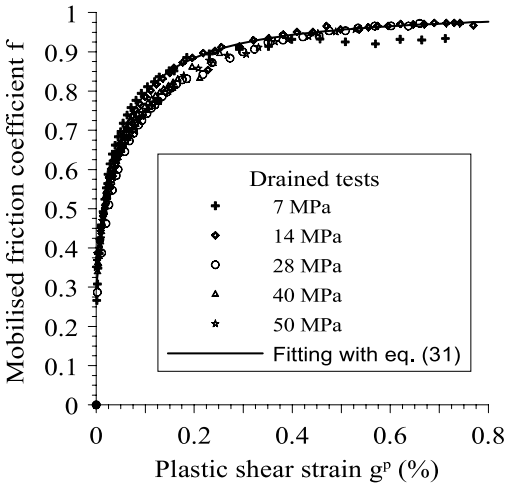

Fig. 15. Drained tests: Mobilised friction coefficient

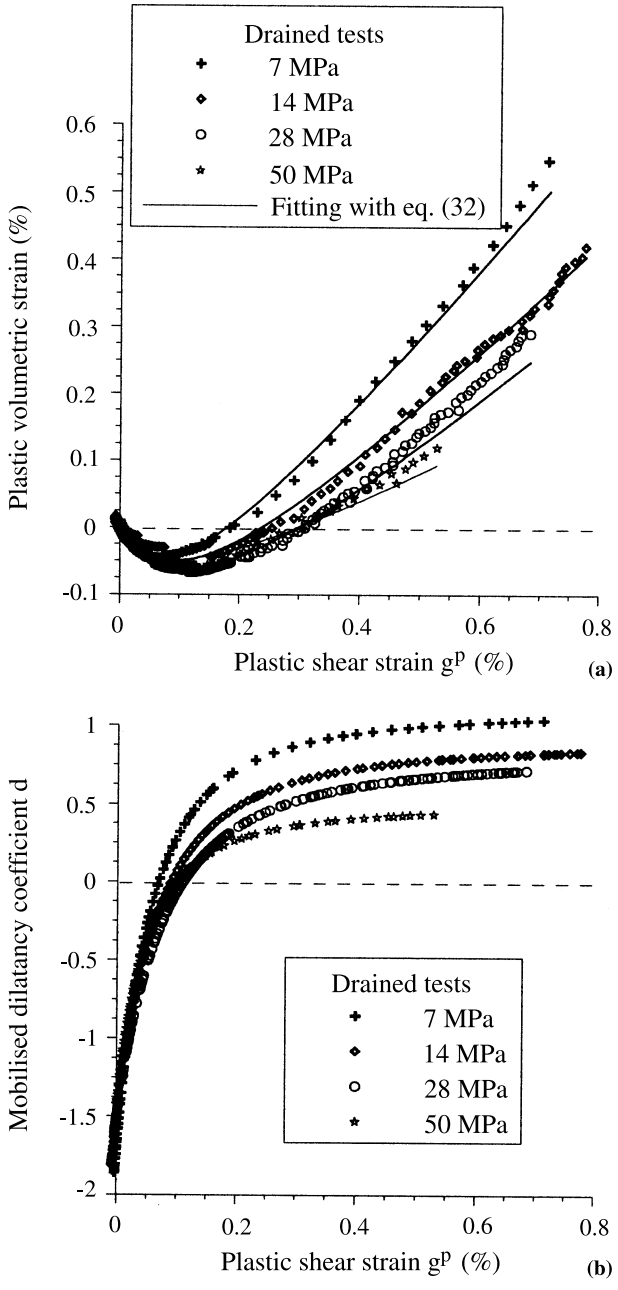

Fig. 16. Drained tests: **a** volumetric plastic strain, **b** Mobilised dilatancy coefficient

The coefficients d_0, d_1, d_2 for the various confining pressures are given in Table 3.

To take into account the pressure-dependent character of the dilatancy coefficient, the dilatancy function is calibrated as a function of both the plastic strain and the

Table 3. Coefficients for the calibration of the plastic volumetric strain function (Eq. (32))

Confining pressure (MPa)	d_1	d_2	d_3
7	−1.7	938	861
14	−1.5	630	710
28	−1.5	500	629
50	−1.4	474	978

effective mean stress p′. We obtain

$$
\begin{aligned}
d_c(p', g^p) &= d^*(g^p)\xi_e(p') \\
d^* &= d_0^* + \frac{(g^p)^2}{d_1^* + d_2^* g^p + d_3^* (g^p)^2} \\
d_0^* &= -1.7;\ d_1^* = 4.1 \times 10^{-8}; d_2^* = 1.8 \times 10^{-4}; d_3^* = 0.35 \\
\xi(\mathrm{p}') &= \left(1 + \frac{p'}{p_1}\right)^N; \quad p_1 = 153.4\,\mathrm{MPa};\ N = 0.4.
\end{aligned} \tag{32}
$$

5.5 Back Analysis of Triaxial Tests

The above elasto-plastic model is validated through the simulation of triaxial compression in drained and undrained conditions and the comparison of the simulation with the actual data.

5.5.1 Simulation of Drained Triaxial Tests

For drained triaxial compression tests the results are shown on Fig. 17 where computed stress-strain curves are plotted for the various confining pressures and compared with the experimental data in the pre-peak regime. Obviously the above model reproduces very satisfactorily the actual data for the slope of the curve and the peak stress.

5.5.2 Simulation of Undrained Triaxial Tests

For the undrained tests, the simulation is performed using the model parameters calibrated on the drained tests. For the computation of the pore pressure generation, the analysis developed in Section 3.2 for elastic behaviour is generalised here to elasto-plastic response. Equation (5) becomes

$$
n\frac{\Delta u}{K_w} + (1-n)\frac{\Delta p'}{K_s} = \Delta\varepsilon_v \tag{33}
$$

with

$$
\begin{aligned}
\Delta p' &= \Delta p - b\Delta u \\
\Delta\varepsilon_v &= \Delta\varepsilon_v^e + \Delta\varepsilon_v^p = \frac{\Delta p'}{K} + \Delta\varepsilon_v^p.
\end{aligned}
$$

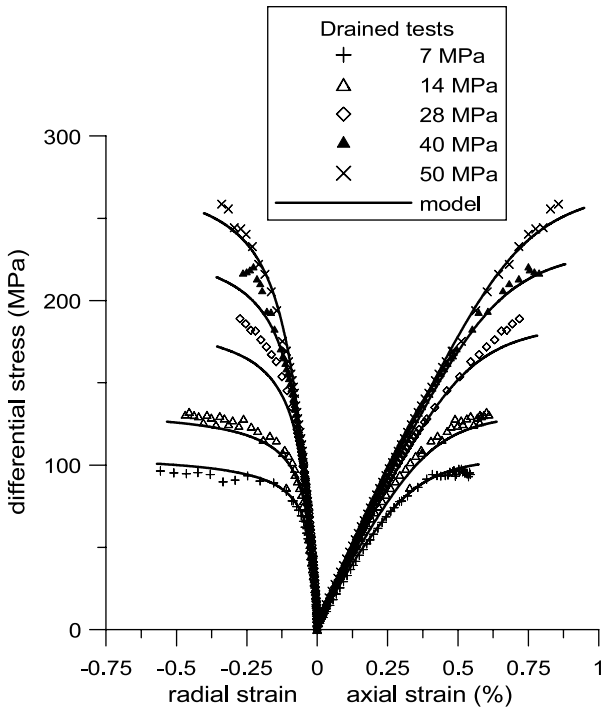

Fig. 17. Drained triaxial compression: Computed and experimental stress-strain curves

The generated pore-pressure can then be evaluated incrementally as follows.

$$\Delta u = \frac{\left(\frac{1}{K} - \frac{1-n}{K_s}\right)}{\left(\frac{n}{K_w} - b\frac{1-n}{K_s} + \frac{b}{K}\right)}|\Delta p| - \frac{\Delta\varepsilon_v^p}{\left(\frac{n}{K_w} - b\frac{1-n}{K_s} + \frac{b}{K}\right)}$$
$$= B|\Delta p| - \frac{\Delta\varepsilon_v^p}{\left(\frac{n}{K_w} - b\frac{1-n}{K_s} + \frac{b}{K}\right)}. \tag{34}$$

It is well known that the effective stress is linked to the constitutive law. Extensive discussion can be found in Coussy (1995). In the poroelastic case, it can be demonstrated that the Biot's effective stress is relevant (Nur and Byerlee, 1971). In the plastic range, although the validity of the effective stress tensor cannot be assessed for any yield criterion, Terzaghi's effective stress is relevant for pressure independent plastic criterion (Von Mises for instance) (Lydzba and Shao, 2002). For pressure-dependent yield criterion such as Mohr Coulomb a generalised effective stress is proposed by De Buhan and Dormieux (1996) and Lydzba and Shao, (2002). In the computations, the Biot's effective stress is used in the elastic domain and the Terzaghi's expression for the effective stress ($b = 1$) is used in the plastic domain in order to keep the model simple. As shown in the numerical simulations, this assumption is acceptable.

The results of the simulation of undrained triaxial tests at various confining pressures are shown on Fig. 18a for the stress-strain response and Fig. 18b for the pore pressure

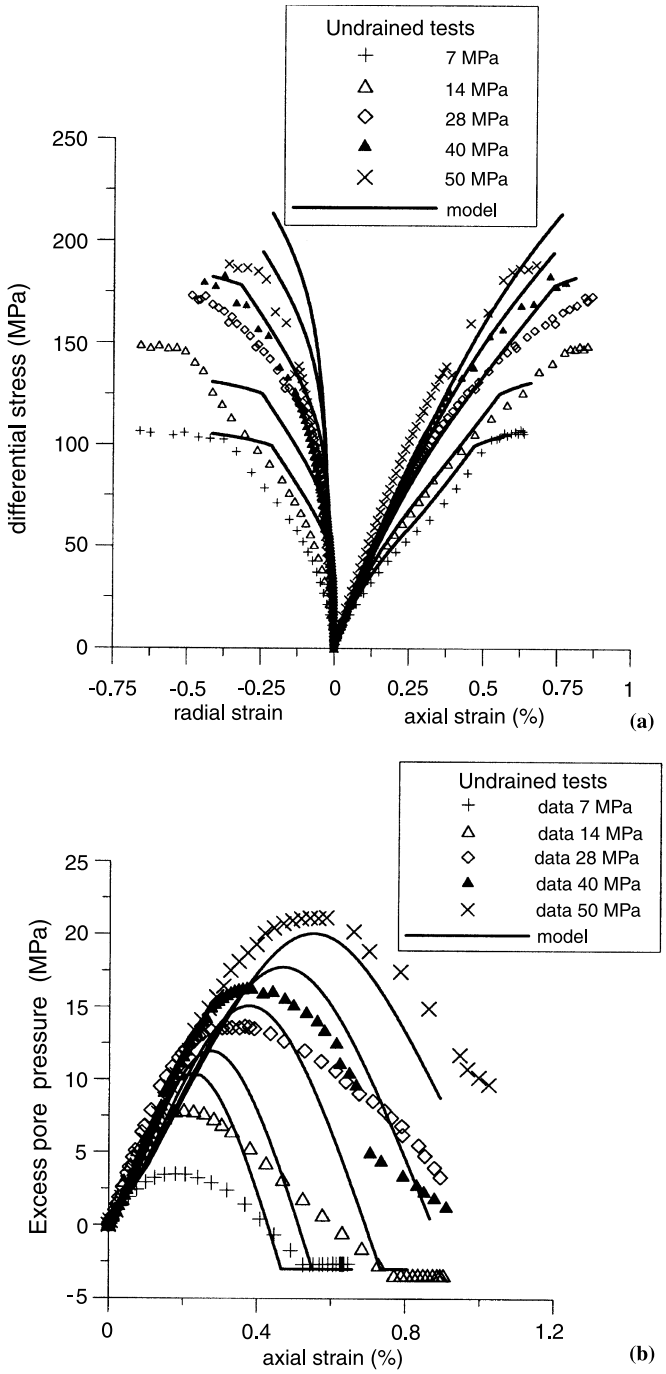

Fig. 18. Undrained triaxial compression: Computed and experimental stress-strain curves **a** and pore pressure evolution **b**

evolution. These graphs show that the experimental data can be reasonably reproduced with the constitutive model proposed. We observe that the computed pore pressure is overestimated at low confining pressures. This could be improved in the future.

6. Conclusion

On the basis of an extensive experimental program of axisymmetric hydrostatic and triaxial compression tests in drained and undrained conditions, the poro-mechanical behaviour of Fontainebleau sandstone is analysed and modelled within the frame of the theory of poro-elastoplasticity. New experimental advances in monitoring pore pressure and strains have allowed to obtain reliable experimental data both for drained and undrained tests. Hydrostatic undrained compression tests have shown the pressure-sensitivity character of the Skempton coefficient B for a sandstone with a relatively high porosity. This has been related to the pressure sensitivity of the bulk modulus of the rock. Accordingly a new expression for the Skempton coefficient B is proposed as a function of the porosity, the drained bulk compressibility and the grain and fluid compressibility and validated through comparison to the experimental data.

The constitutive model developed emphasises the non-linear elasticity of granular rocks through a consistent formulation of stress-dependency and damage and the pressure sensitive plastic behaviour through a friction-hardening non-associated model. The calibration procedure has been presented in details and the back analysis of drained and undrained tests has shown that the experimental results can be satisfactorily reproduced with this model. In particular the maximum pore pressure observed in undrained tests at the critical state of transition between contractant and dilatant volumetric strain is well reproduced by the model as well as the cavitation phenomenon observed at the end of the test at low confining pressure.

Acknowledgements

The authors wish to thank François Martineau (Laboratoire Central des Ponts et Chaussées, Paris) for his assistance in the testing program.

References

Archambault, G., Poirier, S., Rouleau, A., Gentier, S., Riss, J. (1999): Pore pressure behaviour in undrained shear tests on joints. In: Proc. Int. Congress. Rock Mech. 741–745.

Boozer, G. D., Hiller, K. H., Serdengecti, S. (1962): Effects of pore fluids on the deformation behaviour of rocks subjected to triaxial compression. Proc. 5th Symp. Rock Mech., Minneapolis, 579–624.

Bourbie, T., Zinszner, B. (1985): Hydraulic and acoustic properties as a function of porosity in Fontainebleau sandstone J. Geophys. Res. 90(B13), 11524–11532.

Bouteca, M., Guegen, Y. (1999): Mechanical properties of rocks-pore pressure and scale effects. Oil and gaz science and technology. Revue de l'Institut Français du Pétrole 54(6), 703–714.

Bishop, A. W. (1973). The influence of an undrained change in stress on the pore-pressure in porous media of low compressibility. Géotechnique 23(3), 435–442.

Cornet, F. (1977): Etude du comportement élastique et fragile des roches saturées par un liquide. Rev. Franç. Géotechn. 2, 81–100.

Coussy, O. (1995): Mechanics of porous continua. Wiley, New York.

de Buhan, P., Dormieux, L. (1996): On the validity of the effective stress concept for assessing the strength of saturated porous materials: a homogenization approach. J. Mech. Phys. Solids 44, 1649–1667.

David, C., Darot, M. (1989): Permeability and conductivity of sandstones. In: Maury & Fourmaintraux (eds), Rock at great depth. Balkema, Rotterdam, 203–209.

Dropek, R. K., Johnson, J. N., Walsh, J. B. (1978): The influence of pore pressure on the mechanical properties of Kayenta sandstone. J. Geoph. Res. 83(B6), 2817–2824.

El Bied, A., Sulem, J. (2003): Adaptation du mode opératoire pour la réalisation d'essais en compression ≪vraie≫ sur les roches. Rev. Franç. Géotechn. 103, 43–60.

El Bied, A., Sulem, J., Martineau, F. (2002): Microstructure of shear zones in Fontainebleau sandstone, Int. J. Rock Mech. Min. Sci. 39(7), 917–932.

Fabre, D., Gustkiewicz, J. (1997): Proelastic properties of limestones and sandstones under hydrostatic conditions. Int. J. Rock Mech. Min. Sci. 34(1), 127–134.

Fredrich, J. T., Greaves, K. H., Mertin, J. W. (1993): Pore geometry and transport properties of Fontainebleau sandstone. Int. J. Rock Mech. Min. Sci. Geomech. Abstr. 30(7), 691–697.

Fredrich, J. T., Mertin, J. W., Clayton, R. B. (1995): Induced pore pressure response during undrained deformation of tuff and sandstone. Mech. Mater. 20, 95–104.

Garg, S. K., Nur, A. (1973): A. Effective stress laws for fluid saturated porous rocks. J. Geoph. Res. 78(26), 5911–5921.

Gustkiewicz, J. (1998): Compressibility of rocks with special consideration given to pore pressure. In: Thimus et al., (eds), Poromechanics. Balkema, Rotterdam, 573–577.

Haied, A., Kondo, D. (1997): Strain localization in Fontainebleau sandstone : macroscopic and microscopic investigations Int. J. Rock Mech. Min. Min. Sci. 34(3–4) Paper No. 161.

Handin, J., Hager, R. V., Friedman, M., Feather, J. N. (1963): Experimental deformation of sedimentary rocks under confining pressure: pore pressure tests. Bull. Am. Assoc. Petroleum Geologists 47(5), 717–754.

Labuz, J. F., Bridell, J. M. (1993): Reducing frictional constraint in compression testing through lubrication. Int. J. Rock Mech. Min. Sci. Geomech. Abstr. 30, 451–455.

Lade, P. V., De Boer, R. (1997): The concept of effective stress for soil, concrete and rock. Géotechnique 47(1), 61–78.

Lane, K. S. (1970): Engineering problems due to fluid pressure response in rock. Rock Mechanics – Theory and practice. Am. Inst. Pet. Eng., Univ. California, 501–514.

Lemaître, J. (1990): A course on damage mechanics. Springer, Berlin Heidelberg New York, Tokyo.

Loret, B. (1985): On the choice of elastic parameters for sand. Int. J. Num. Anal. Meth. Geomech. 9, 285–292.

Lydzba, D., Shao, J. F. (2002): Stress equivalence principle for saturated porous media. C.R. Acad. Sci. Paris, Mécanique 330, 297–303.

Merritt, J., Aldrich, M. J. (1969): Pore pressure effects on Berea sandstone subjected to experimental deformation. Geol. Soc. AM. Bull. 80, 1577–1586.

Mesri, G. K., Adachi, K., Ullrich, C. R. (1976): Pore-pressure response in tock to undrained change in all-round stress, Géotechnique 26(2), 317–330.

Nur, A., Byerlee, J. D. (1971): A exact effective stress law for elastic deformation of rock with fluids, J. Geoph. Res. 76, 6414–6419.

Papamichos, E. (1999) Constitutive laws for geomaterials, Oil Gas Sci. Technol. 54(6), 759–771.

Papamichos, E., Tronvoll, J., Skjaestein, A., Unander, T. E., Labuz, J. F., Vardoulakis, I., Sulem, J. (2000): Constitutive testing of a weak sandstone. Mech. Cohes. Frict. Mater. 5, 1–40.

Pellegrino, A., Sulem, J., Barla, G. (1997): The effect of slenderness an lubrication on the uniaxial behavior of a soft limestone. Technical note. Int. J. Rock Mech. Min. Sci. 34(2), 333–340.

Robinson, L. H. (1959): The effect of pore and confining pressure on the failure process in sedimentary rock. 3rd Symp. Rock Mech. Colorado School of Mines, 371–394.

Roger, V., Desrues, J., Viggiani, G. (1998): Experiments on strain localisation in dense sand under isochoric conditions. In: Oka, F. (ed.), Localisation and bifurcation theory for soils and rocks. Balkema, Rotterdam, 239–248.

Streiger, R. P., Leung, P. K. (1991): Consolidated undrained triaxial test procedure for shale. In: Roegiers, J. C. (ed.), Rock mechanics as a multidisciplinary science. Proc. 32nd U. S. Symp., Balkema, Rotterdam, 637–646.

Sulem, J., Vardoulakis, I., Papamichos, E., Oulahna, A., Tronvoll, J. (1999): Elasto-plastic modelling of Red Wildmoor sandstone. Mech. Cohes. Frict. Mater. 4, 215–245.

Taylor, D. W. (1948): Fundamentals of soil mechanics, J. Wiley, New York.

Tien,Y. M., Lee, D. H., Juang, C. H. (1988): A study on the strain and pore water pressure characteristics of sandstone during repeated loading. In: Cundall et al., (eds). Key questions in rock mechanics, Balkema, Rotterdam, 43–49.

Vardoulakis, I., Sulem, J. (1995): Bifurcation analysis in geomechanics. Blackie Academic and Professional, London.

Zimmerman, R. W. (1991): Compressibility of sandstones. Elsevier, Amsterdam.

Authors' address: Dr. Jean Sulem, CERMES, Ecole Nationale des Ponts et Chaussées, 6 et 8 avenue Blaise Pascal, Cité Descartes, Champs-sur-Marne, 77455, Marne-La-Vallée, cedex 2, France; e-mail: sulem@cermes.enpc.fr